Single Image Super-Resolution Enhancement using Luminance Map and Atmospheric Light Removal

S. Poormajidi[1] , M. A. Shayegan[2*]
1- Department of Computer, Shiraz Branch, Islamic Azad University, Shiraz, Iran.
Email: smajidi6029@gmail.com
2- Department of Computer, Shiraz Branch, Islamic Azad University, Shiraz, Iran.
Email: MA.Shayegan@iau.ac.ir (Corresponding Author)

Received:3 September 2022 Revised: 28 September 2022 Accepted: 31 October 2022

ABSTRACT:
Super resolution algorithms attempt to reconstruct high resolution images from low resolution images and it can be considered as a preprocessing step for object recognition and image classification. Various algorithms have been introduced for single-image super resolution, but these algorithms often face important challenges such as poorly matching the reconstructed image with the original image. This article introduces a preprocessing operation to improve the performance of the super resolution process. In the proposed method, the low-resolution images are enhanced before entering to the resolution change module. Calculating the brightness of the pixels in the image channels, creating the luminance map and removing atmospheric light, applying the transmittance map by using the luminance coefficients, and recovering the natural image in all three-color channels are the above preprocessing steps. The proposed method succeeded in increasing the PSNR parameter by 4.35%, 10.62%, and 8.31%, as well as 0.23%, 3.10%, and 7.91% of the SSIM parameter for Set5, Set14, and BSD100 benchmark datasets compared to its closest state-of-the-art methods.

KEYWORDS: Single Image Super Resolution, Natural Images, Luminance Map, GAN, Convolutional Neural Network.

1. INTRODUCTION

Nowadays, the use of digital cameras that can capture and store images with different resolutions has become very common. With the advancement of image processing science and its development in various fields, such as visual communication and scene perception, the need for high spatial resolution images has increased, because these images provide better and more detail to identify the scene [1].

Image resolution, in terms of hardware, depends on the capabilities of the imaging devices. Hence, to increase the resolution of the images by the hardware, the pixel size should be reduced or the sensor chip capability should be increased by using expensive hardware. However, signal processing software techniques can be used to produce low-cost High Resolution (HR) images [2]. These algorithms have overcome and compensated for the limitations and shortcomings of video recording hardware or adverse environmental conditions and therefore have received much attention.

The Super Resolution (SR) technique enables users to go beyond the capabilities of the imaging systems. In this technique, an HR image is generated using one or more Low Resolution (LR) images. HR images play an important role in many fields, including satellite imaging, aerial photography, ultrasound, medicine, traffic monitoring, security monitoring, earth-observation remote sensing, astronomical observations, biometric information detection, and so on [3].

SR algorithms are implemented in both software and hardware methods. In the hardware method, the resolution is increased with changes in the structure of the camera sensors. However, this method is not a universal method due to the high-cost of implementation and the limitations in the technology of manufacturing parts. In contrast, the software methods are cost-effective and an LR image is converted to an HR image without changing the camera structure.

According to the number of input images, the SR techniques are divided into two categories: Single Image Super Resolution (SISR) and Multi Image Super Resolution (MISR) techniques [4]. The SISR techniques access only one image to create an HR image, while MISR techniques access multiple images

Paper type: Research paper
DOI: 10.30486/mjee.2022.696516
How to cite this paper: S. Poormajidi and M. A. Shayegan, "Single Image Super-Resolution Enhancement using Luminance Map and Atmospheric Light Removal", Majlesi Journal of Electrical Engineering, Vol. 16, No. 4, pp. 37-59, 2022.

and combine images information to create an HR image to get deep image features.

SR methods are generally divided into three main categories: interpolation, reconstruction, and learning methods [5]. However, interpolation methods have been extensively studied. In these methods, each pixel of an HR image is obtained by calculating the weighted average of the adjacent pixels in an LR image. Interpolation-based algorithms in SISR, including Nearest Neighborhood, Bilinear, and Bicubic, cause the image to blur and indented. However, by using sharpening methods and prior knowledge of the edges, the abnormal artifacts of the images can be reduced to some extent, but these methods still cannot improve the details of the image, properly.

Reconstruction methods use LR image information such as local texture and gradient due to the unavailability of the HR image. These methods provide better results for HR image reconstruction, but with an increasing magnification factor, the image quality decreases, quickly [6].

In recent years, learning methods have attracted a lot of attention due to overcoming the problems in this field. These methods establish the relationship between the HR and LR images as a prerequisite for output reconstruction. These methods improve and sharpen the edges of the image, but they have a high computational cost.

The most important challenges in the field of SISR include the following: Loss of high-frequency image detail [5]; Blurred motion in the images [7]; Low spatial resolution in images [8]; Loss of sharp edges and edge details in SR reconstructed images [9]; Failure to maintain the image structure during up-sampling and increasing the noise [10], and poor performance in the presence of noise in the original images [11].

The main contribution of this article is introducing a preprocessing method for LR input images. This preprocessing method includes calculating the brightness of the pixels in the image channels, creating the luminance map and removing atmospheric light, applying the transmittance map taking into account the luminance coefficients, and recovering the natural image in all three colors channels. It prevents the smoothing of the images which has a great effect on improving the SISR process.

The following sections of this article are organized as follows. Section 2 expresses the theoretical foundations related to the subject as well as research records in this field, and it briefly introduces some SR methods. Section 3 introduces the proposed method and its implementation steps. In section 4, the experiments and results are introduced and finally, section 5 compares the results with other SR methods.

2. LITERATURE REVIEW

2.1. The Theoretical Background

2.1.1. Super Resolution

SR is an algorithm in which one or more LR input images are received and an HR image is generated at the output [12]. The general framework of SISR algorithms is shown in Fig. 1 [13].

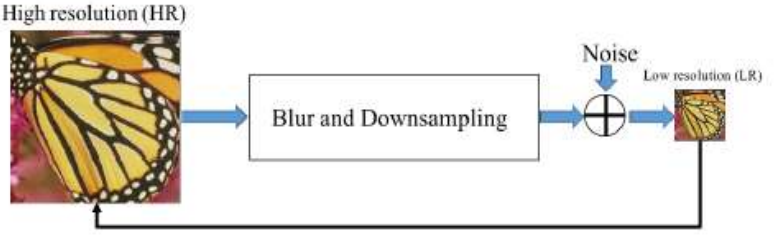

Fig. 1. General SISR framework [13].

As shown in Fig. 1, an HR image is converted to a corresponding LR image using down-sampling and blurring, as well as the addition of noise. As a result, it is tried to convert the LR image to the original HR image using SISR methods. An LR image is often modeled as Equation 1:

$$y = (x \otimes k) \downarrow_s + n \quad (1)$$

In Equation 1, the variable x is the LR image and the variable k is the blurring core multiplied by the input image. The symbol $\downarrow_S$ is the down-sampling operation with the scale factor *s* and the variable *n* is the added noise to the input image [13].

2.1.2. Light Scattering Model in Natural Images

Atmospheric light refers to rays in nature that causes the image of objects to appear in the human eyes. The color intensity of each ray of light in nature has a certain amount of energy, which is represented as Equation 2 [14]:

$$\mathrm{E}_{\mathrm{W}}^{\mathrm{c}}(x) = \mathrm{E}_{\mathrm{A}}^{\mathrm{c}}(x) + E^{n}(x), c \in \{r, g, b\} \quad (2)$$

In Equation 2, $E_W^c(x)$ is the amount of pixel brightness x after imaging, $E_A^c(x)$ is the amount of atmospheric light in all three-color channels R, G, B, and $E^n(x)$ is the amount of noise in the image. According to the above, the main image in natural images is defined as Equation 3 [14]:

$$I^c(x) = J^c(x)T^c(x) + \big(1 - T^c(x)\big)A^c \quad , \quad c \in \{r, g, b\} \tag{3}$$

In Equation 3, $J^c(x)$ is the original image without artificial light, $T^c(x)$ is the pixel transmittance map x, and A^c is the brightness range. One way to select the amount of atmospheric light is to use the maximum color intensity in the image. To do this, 0.1% of the maximum brightness of the image in the dark channels of the image (or image brightness map) is selected, firstly. Then, the pixels corresponding to this value are found in the main image and the maximum brightness of those pixels is selected as the atmospheric light of the image [15]. However, one of the problems with this method is the presence of some bright objects in the input image whose color intensity is more than the atmospheric light, which prevents the extraction of the original natural image, correctly. One of the reasons for this phenomenon is the flash of cameras and environmental factors such as high-intensity light sources.

One solution to overcome the atmospheric light problem is to remove bright areas in the image with low-pass filters, which balances the bright color spectra in the image. Therefore, the brightness of each x pixel is modeled as Equation 4 [14]:

$$I^c(x) = E_w^c(x).R(x) \tag{4}$$

In Equation 4, R(x) is a distribution function that indicates the reflection of light in the environment. Due to the difficulty of estimating the value of this function, it is usually considered constant. Thereafter, noise removal filters are used to balance the brightness. After removing the high light intensity sources, a value for the light intensity can be considered.

2.1.3. Generative Adversarial Networks (GANs)

An important group of Deep Neural Networks (DNNs) is generative models. The purpose of the generative model is to learn the density function that describes the original sample data. It then uses this estimated density to generate real data similar to the original sample. GANs have been used in various applications such as video frame prediction, image resolution enhancement, new data generation, and data modification [16].

Fig. 2 shows the general structure of the GAN networks. These networks consist of two parts. The first part is the Generative (G) network which aims to learn the P_x distribution that is consistent with the target data. The second part is the discriminative (D) network, which aims to learn the difference between the real data and the data produced by the G network. The training method of G and D networks is shown in Fig. 3.

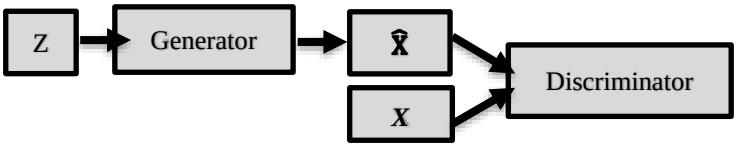

Fig. 2. General structure of the GAN networks [16].

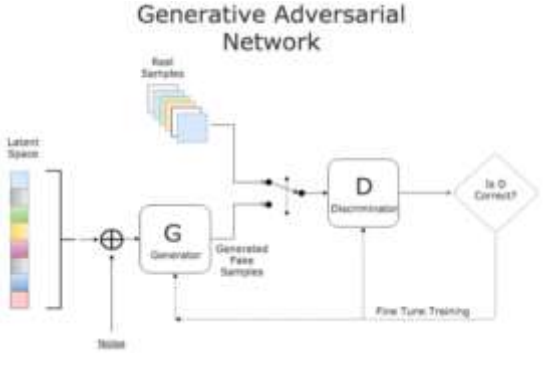

Fig. 3. GAN network training [16].

The two G and D networks compete and train in a minimum-maximum competition [16]. In a GAN network, noise is first sampled from the latent space, and that sample is given to the G network as the initial image to create new data. On the other hand, there are real data, too. At each stage, one of the fake or real images enters the D network. Network D is trained to determine whether data is real or not. If network D detects unreal data, network G will be trained again. This process continues until the D network cannot detect that the input data is real or fake.

2.1.4. Image Quality Assessment (IQA)

IQA criteria calculate the difference between the input image and the SR image [17]. IQA methods are divided into subjective and objective groups. Subjective methods operate based on the human visual system and are therefore a reliable tool for assessing quality. However, due to their time-consuming and costly nature, they are rarely used for practical applications. To overcome these limitations, other image-based criteria have been proposed to predict the human perception of image quality, which are objective methods [17]. The following are some important IQA parameters [18].

- *Structural Similarity Index Measure (SSIM)*

SSIM provides a good approximation for measuring image quality by measuring the structural similarity between the input image and the SR image. For the two images A (reference image) and B (reconstructed image), the SSIM is defined as Equation 5 [18]:

$$\mathrm{SSIM}(\mathbf{A},\mathbf{B}) = \frac{(2\mu_a\mu_b + C_1)(2\sigma_{ab} + C_2)}{(\mu_a^2\mu_b^2 + C_1)(\sigma_a^2 + \sigma_b^2 + C_2)} \quad (5)$$

In Equation 5, μ_a and μ_b are the local mean of the A and B images, σ_a and σ_b are the standard deviations of the A and B images, σ_{ab} is the covariance of the two images, and C_1 and C_2 are constant values. The value of the SSIM varies between 0 and 1. A value of zero indicates the complete dissimilarity of the reconstructed image with the original image and a value of 1 indicates the complete correlation of the reconstructed image with the original image. Therefore, a higher SSIM value will indicate better quality of the reconstructed image.

- *Mean Square Error (MSE)*

Equation 6 shows the MSE, where $A_{i,j}$ are the original image pixels, $B_{i,j}$ are the reconstructed image pixels, and M and N are the dimensions of the images A and B.

$$\mathrm{MSE} = \frac{\sum_{j=1}^{N}(\sum_{i=1}^{M}(A_{i,j} - B_{i,j})^2)}{\mathrm{MN}} \quad (6)$$

- *Peak Signal to Noise Ratio (PSNR)*

The PSNR criterion is the ratio between the maximum powers of a signal to the amount of noise that affects the image appearance quality. Therefore, a larger PSNR indicates the quality improvement of the reconstructed image (Equation 7) [18].

$$\mathrm{PSNR} = 10\log_{10}\frac{(\text{maximum pixel value})^2}{\mathrm{MSE}} \quad (7)$$

2.2. Related Works

In the following, some proposed methods in this field have been introduced in the form of several general groups.

2.2.1. Sparse Representation Technique

Some researchers have used spars display techniques to improve the quality of the SR images. Harris et al. introduced a spars display-based SR algorithm to reduce the blurring of images obtained from unmanned aerial vehicles [4]. In the proposed method, multiple pairs of HR and LR image dictionaries are matched using the edges of images to select the best appropriate dictionary pair for a particular image. In this study, 5 pairs of HR and LR dictionaries were generated and used in the spars coding step to create an enhanced image. Qualitative and quantitative analysis of the proposed method show the reduction of opacity and removal of excess color artifacts, especially in the edge areas of remote sensing images. However, this method is very time-consuming.

It is very difficult to find sparse representation for remote sensing images, due to their texture and edge characteristics. However, Li et al. introduced an SR algorithm using Mixed Sparse Representation (MSR) to segment remote sensing sub-images, such as smooth components and dot-and-edge-like components [19]. In the proposed MSR method, an HR image is obtained using wavelet transforms. Experimental results show about 5% improvement in MSR classification accuracy. It also produces higher resolution images than other conventional SR methods.

2.2.2. Point Spread Function (PSF) estimation

For increasing the quality of remote sensing images, Fan et al. introduced an SR algorithm based on estimating the PSF of LR remote sensing images [20]. The proposed method consists of three steps: LR image estimation with linear interpolation; calculating the displacement of LR image pixels via SR operation, and repeating the second step until convergence. The most important advantage of the proposed method is the enhancement of the spatial resolution of the image. The experimental results show that the PSF is improved in LR images with increasing computational time.

Intending to produce HR images from LR satellite images, LV et al. proposed a method for capturing images and estimating PSF [21]. The proposed model

optimally combines the two parts; i.e. PSF estimation and image capture. One of the strengths of the proposed method is its efficiency on artificial and real data, and one of the weaknesses of that is more computation time compared with current methods. The results showed that the accuracy of this method increased by approximately 1% on SPOT-5 and ALOS-PRISM satellite images datasets.

2.2.3. Noise Removal

Bei et al. introduced the Denoising for Super Resolution (DNSR) model to eliminate image noise during up-sampling and the Automated Decomposition and Reconstruction for Super Resolution (ADRSR) model to maintain image structure [10]. In the proposed method, the PSNR value was equal to 24.90 and the SSIM value was equal to 0.7956 on the DIV2K dataset, which was slightly higher than the competing methods. The advantage of this method is the improvement of the sharpness of images edges and one of its disadvantages is the long computational time.

An HR image is essentially a structure that includes a matte image as a mask. Therefore, extracting the mask using noise removal methods is essential. By considering this fact, Brifman et al. presented a SISR method based on noise removal algorithms [11]. They employed Gaussian-shaped filters for the noise removal task. However, one of the disadvantages of Gaussian filters is that they do not pay attention to the zero-crossing points, which causes the image edges disappearance. As a result, combining several Gaussian mixed functions and finally calculating the maximum similarity between these functions, has caused the challenge to be partially solved.

2.2.4. Self-Similarity

Cruz et al. developed a Patch-based SR algorithm based on Self-Similarity to improve the resolution of single images [22]. Current patch-based methods use external data to obtain similar patches. However, in this research, a large group of extracted similar patches from the input image is used, and large external data are no longer needed. The proposed method obtains similar patches with the Euclidean distance criterion, in the first step. Then, it uses a 1D Wiener filter to estimate the SR image. The results show higher sharpness, image clarity as well as less computation. In the proposed method, the PSNR values were obtained 31.39 and 27.98 by using Set5 and Set14 databases, in order.

2.2.5. Deep Networks

To improve the sharpness of natural images, Lin et al. proposed a SISR algorithm based on unsupervised deep learning, using a GAN framework [23]. The proposed method combines a deep convolution compact connections G network (which is trained to enhance the HR image of an LR image) and a D network (to distinguish HR images from HR images generated by the generator) with a ReLU activation function. A Sub-Pixel convolution layer has been used in the G network to up-sample input images. In the proposed method using the Set5 database, the values of PSNR and SSIM were 30.42 and 0.8594, respectively.

Ledig et al. noted that the use of deep networks, while increasing the accuracy and speed of existing SISR algorithms, still have difficulty recovering image texture details during up-sampling operation [24]. Those researchers said that the reason for the mentioned problem is the specific choice of the objective function in optimized SR algorithms. These algorithms often focus on minimizing image reconstruction error. Therefore, these methods achieve high values for the PSNR parameter, but reduce the high-frequency information of the images as well as the small details of the image texture. This problem reduces the visual perception of the image.

Referring to the above problem, these researchers introduced the Super-Resolution Generative Adversarial Network (SRGAN) algorithm whose loss function is a perceptual loss function. The SRGAN consists of an adversarial loss function and a content loss function. The adversarial loss function leads the algorithm to produce a natural image corresponding to the real images. The content loss function brings the image closer to the real image at the content level instead of the pixel level. The above algorithm, by using the VGG54 deep network, achieved values of 29.40, 26.02, and 25.16 for the PSNR parameter and values of 0.8472, 0.7397, and 0.6688 for the SSIM parameter for the Set5, Set14, and BSD100 databases, respectively.

Zhang et al. used conditional GAN (CGAN) to generate SISR images [25]. For better large-scale image reconstruction, they designed an Enhanced Laplacian Pyramid Network (ELapN) as a generator in CGAN, which gradually reconstructs HR images across several pyramid levels. ELapN extends low-level and high-level features for residual image learning better than those based solely on high-level information. The proposed network was trained using a combination of CGAN and VGG to achieve high-quality SR results. The results for the databases Set5, Set14, and B100 show the superiority of the proposed method over some current methods in terms of PSNR and SSIM.

To eliminate visual artifacts created during the SR process by the GAN network, Qiao et al. used ground-truth information from early HR images to better train the GAN network [26]. In the designed GAN network, the low-level and high-level features are integrated through the compact connections of the residual blocks, in different layers. Their proposed method produced

better PSNR and SSIM compared to competitors as well as better results in terms of visual perception.

Chen et al. introduced a dual-driven GAN network, which is called Guided Dual Super Resolution (GDSR) [27]. GDSR network has two important modules. The first module extracts general and visual features from LR images and the second module focuses on extracting and learning the small and unique details of the image. Experiments performed by this researcher on standard databases Set5, Set14, BSD100, Urban100, and Manga showed the superiority of the above method over some competing methods in this field.

To show the dependencies of LR and HR images, Haris et al. introduced a Deep Back Projection Network (DBPN) for the SISR task [28]. The proposed method includes three stages including initial feature extraction, projection, and reconstruction. Features are extracted by using two layers of convolution. Feature maps are then created using the up-projection and down-projection units. Finally, all feature maps are connected and a final SR image is created with a layer of convolution. The databases Set5 and Set14 were used in this research. The PSNR values were 31.59 and 28.21 using in the Set5 and Set14, in order.

To preserve important features in a SISR process, Hu et al. proposed a network that combined spatial features with channel-wise features [29]. The proposed method consists of three modules: initial feature extraction, feature conversion, and subnet up-sampling. In the proposed method, an LR input image is displayed as a set of feature maps. The feature conversion section is also used to convert shallow features to deep features. In the proposed method, the PSNR value was 32.06 and the SSIM value was 0.9462 for the Urban100 database, which showed an improvement compared to other existing methods.

Xu and Li proposed a SISR algorithm based on Spatial Color Attention Networks (SCAN) for R, G, and B channels of color images [30]. In the first step, the LR image passes through one convolution layer. Thereafter, the image is reconstructed using three Basic_RGM modules, and the output again passes through two convolution layers. In the second step, the LR image is converted to three color channels R, G, and B using the SCAM module. In the third stage, the outputs of the first and second stages are added to the input LR image to create the HR image. In this research, the NTIRE2019 database was used and the value of 29.37 for PSNR was obtained that it showed an improvement in performance in terms of visual quality.

Gao and Zhuang proposed two Multi-Scale Deep Neural Networks (MSDNN) for SISR intending to create SR images with different dimensions [31]. The proposed method can upgrade various upscale factors. Initially, due to the complexity of the computations in the HR space, the input image is processed in two different downscale spaces. This reduces GPU usage and increases feature maps of each layer. Then, to reconstruct the image detail, they designed a Multi-Scale Residual Network (MSRN) in the downscale spaces, which expands the layers of convolution. In addition, the researchers proposed a Multi-Scale Dense Network (MSDN) based on dense blocks for comparison to MSRN that can be used in any space. Experimental results showed that the proposed method would be useful for uncertain and unequal upscale factors. In this method, the PSNR and SSIM values in the MSDN architecture were higher than the MSRN. It should be noted that one of the weaknesses of the proposed method is the loss of information in downscale spaces.

Xie et al. proposed a Convolutional Sparse Coding (CSC) method intending to enhance SISR images [32]. The proposed network consists of 3 stages of component analysis, mapping detection, and reconstruction. In this method, the LR image is first decomposed into two components, smooth and residual. The smooth component is extracted using CSC and the residual component is obtained by subtracting the smooth component from the LR image. In the mapping detection step, the residual component is mapped using interpolation and convolution layers. The smooth component is mapped with just a simple interpolation due to the presence of low-frequency information. Finally, in the reconstruction section, the two components are combined and the final HR image is produced. The results show that the proposed method in terms of visual quality is significantly more accurate than other methods that do not use smooth and residual components. In this study, the PSNR and the SSIM values were 31.30 and 0.8388, respectively by using the Set5 database.

Yang et al. provided a Lightweight Feature Fusion Network (LFFN) for SISR to take full advantage of feature map information [33]. The proposed method includes three steps spindle blocks, Softmax feature integration, and up-sampling. Spindle blocks include 3 parts, dimension expansion unit, feature discovery unit, and feature refining unit. In the dimension expansion unit, the dimensions are expanded from 48 to 64 pixels. The Softmax feature integration step is used to obtain information that is more efficient. One of the strengths of this method is designing the network with fewer parameters compared with rival methods. In this study, the PSNR value was 37.95 and the SSIM value was 0.9597, by using the Set5 database.

Dai et al. proposed a Second-order Attention Network (SAN-based) SISR algorithm using intermediate layer feature communication in CNNs [34]. The proposed method includes 4 steps of shallow feature extraction, deep feature extraction, upscale

operation, and reconstruction. The SAN retains spatial information as well as extracts LR image information and passes low-frequency information. In the proposed method for extracting the shallow feature, only one convolution layer has been used. The proposed method performed better than current methods in terms of visual quality.

Wang et al. proposed a CNN-based SR algorithm to commonly learn a deep network and shallow network in an end-to-end model [35]. The proposed network consists of three steps feature extraction, up-sampling, and image reconstruction, which are performed commonly in both networks. The feature extraction module consists of 3 convolution layers with a Relu activation function. To add the input feature map, the outputs of the second and third layers are connected. The up-sample module connects the output of the feature extraction and reconstruction modules.

The shallow network with poor learning capability reconstructs the main structure of image content, while the deep network retains high-frequency details based on the main image structure, which reduces the difficulty of deep network training. Using a deeper network with more complexity increases the accuracy of the network, but prolongs the training time of the network. To address this challenge, the use of the shallow network simplifies the learning process. One of the strengths of the proposed method is the common training of the two networks, which significantly reduces the difficulty of network training. The proposed model achieved 31.14 for PSNR and 0.8783 for SSIM using the Set5 benchmark dataset.

To make full use of the features of the previous layers, Xu et al. proposed a Dense Feature Fusion Convolution Network (DFFNet) for the SISR task [36]. The proposed method consists of three parts: Coarse Feature Extraction block (CFEblock), Dense Feature Fusion Blocks (DFFBs), and Reconstruction Block (Recblock). This method extracts dense features from an LR image to reconstruct directly an HR image without image scaling preprocessing. The databases Set5, Set14, BSD100, and Urban100 were used in this research. Finally, the values of 32.44 and 0.8949 were obtained for PSNR and SSIM using the Set5 database.

By integrating basic image knowledge into their proposed model, Fang et al. proposed a deep network called SeaNet to reconstruct an SR image [37]. The SeaNet network includes three subnets: Rough Image Reconstruction Network (RIRN), Edge-Net Reconstruction (IRN), and Image Refinement Network (IRN). The reconstruction process consists of two stages. In the first stage, the rough SR and soft edge SR feature maps are reconstructed by the RIRN and Edge-Net networks, respectively. In the second step, the outputs of the previous steps are merged and transferred to the IRN to reconstruct the high-quality SR image. Experiments showed that SeaNet converges quickly and achieves good results. The proposed method achieves SSIM equal to 0.96, 0.91, 0.90, and 0.93 for Set5, Set14, BSDS100, and Urban100 databases, respectively. These results are suitable compared with the existing methods.

3. THE PROPOSED METHOD

The proposed noise removal method in this article will prevent smoothing and loss of edges of images. The proposed method includes the steps:

1: Importing the LR input image to the model;

2: Calculating the brightness of the pixels in the image channels;

3: Calculating the luminance map and removing the atmospheric light;

4: Applying the transmittance map using the luminance coefficients;

5: Recovering the natural image in all three colors channels;

6: Importing the enhanced LR image into the SRGAN network and converting this image to SR image using the ResNet architecture;

7: Evaluating the SR image quality by the D network using the VGG54 architecture; and

8: Testing the ultimate goal of the SR operation.

Fig. 4 describes the details of the mentioned steps.

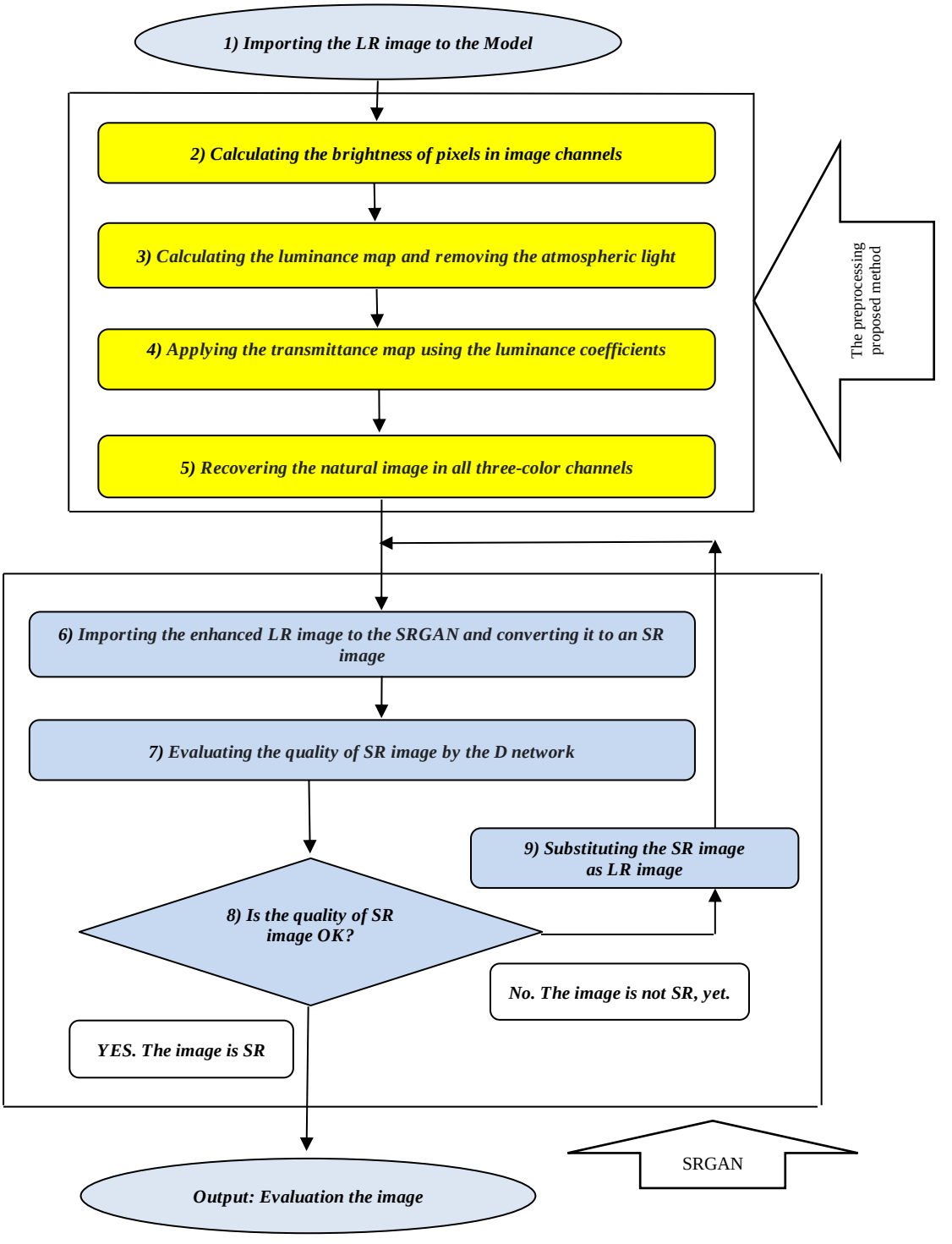

Fig. 4. The proposed model.

3.1. Importing the LR Image to the Model

The proposed method uses three benchmark databases Set5 [38], Set14 [39], and BSD100 [40], which are the most important standard databases in the field. Set5 contains 5 images, one with 512×512 pixels and the other four images with smaller dimensions. Set14 contains 14 images with larger dimensions than Set5. The BSD100 dataset also includes 100 real-life images. Figs. 5, 6, and 7 show the reference images used in this paper from the Set5, Set14, and BSD100 databases, respectively.

Fig. 5. Sample images from the Set5 database [38].

Fig. 6. Sample images from the Set14 database [39].

Fig. 7. Sample images from the BSD100 database [40].

3.2. Calculating the Brightness of Pixels in Image Channels

The proposed pre-processing block includes the second to fifth steps of Fig. 4, which enhances the initial image before the image enters the SRGAN neural network. Enhancement refers to the elimination of the noise that occurs during normal imaging due to the way the aperture of the camcorder works. In the proposed method, using the atmospheric light, an HR image is generated in the preprocessing step.

Atmospheric light is a natural factor that can inadvertently reduce the dynamic range of images contrast. Natural images taken by camcorders have different quality from what is perceived by the human eye. The reason for this problem is the darkening or excessive light of the areas that are exposed to atmospheric light. Hence, in the proposed method, the relatively accurate value of atmospheric light has been obtained, using the concept of dark channels. By doing this, the unwanted image noises will be mostly eliminated [14].

Calculating the exact value of atmospheric light is an important step in the initial producing the HR images. Fig. 8 shows an example of an input image and an image obtained by calculating atmospheric light using dark channels.

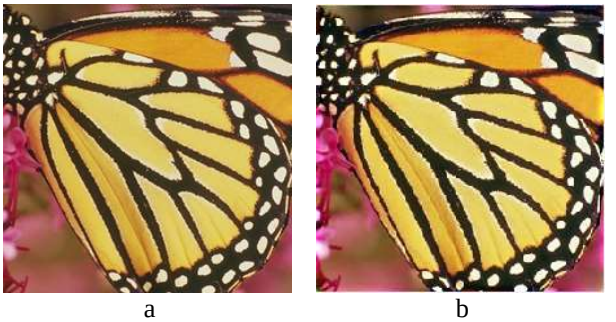

a b

Fig. 8. a) LR input image b) Calculation of atmospheric light using the concept of the dark channels.

3.3. Calculating the Luminance Map and Removing the Atmospheric Light

For the image enhancement task, the input image is mapped to an atmospheric light emission model and then the combination of the three colors channels of the original image is investigated [41]. This process is called calculating the luminance map. In other words, the luminance map shows the saturation of the image in each color channel.

The luminance map acts as a mapping function and obtains the output image based on the color intensity of the input pixels. Before calculating the luminance map, the input image should be reversed (switching light pixels with dark pixels). The reason for this is the high similarity of the obtained outputs with the case when dark channels have been applied to the input images. The equations for the calculation of atmospheric light have been introduced in Section 2-1-2. Fig. 9 shows the artificial light removal on a sample image.

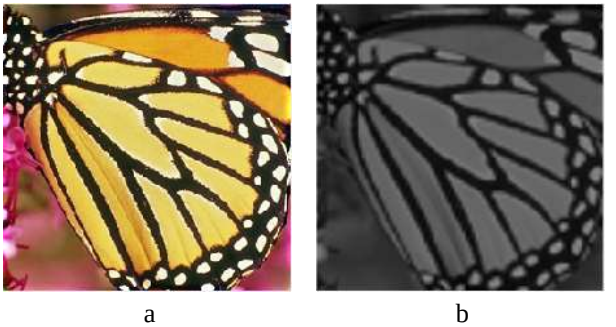

a b

Fig. 9. a) Calculating atmospheric light using the dark channels b) Removing artificial light for the input image.

3.4. Applying the Transmittance Map by Considering the Luminance Coefficients

In the proposed method, the mapping operation is performed without the usual calculations for dark channels, and the initial matrix of the transmittance map is created by Equation 9 [15]:

$$Y(x) = 0.299 \times I_{inv}^{R}(x) + 0.587 \times I_{inv}^{G}(x) + 0.114 \times I_{inv}^{B}(x) \quad (9)$$

In Equation 9, the values $I_{inv}^{R}(x)$, $I_{inv}^{G}(x)$, and $I_{inv}^{B}(x)$ are the components of the R, G, and B channels of the inverted image, respectively. To calculate atmospheric light, 0.1% of the maximum brightness of the image in the image luminance map is selected, firstly. Then, the pixels corresponding to this value are found in the main image and the maximum value of brightness of those pixels is considered as atmospheric light of the image. Then, the transmittance map based on the luminance map is applied to the image (Equation 10) [15]. In this function, Y(x) is the luminance map, and ω is a constant between 0 and 1, depend to the problem.

$$t'(x) = 1 - \frac{\omega Y(x)}{255} \quad (10)$$

This function has advantages over dark channels, which can be mentioned in the high-speed calculations due to the simplicity of the above relationship and the prevention of image artifacts [14]. In addition, environmental changes have little effect on luminance maps, as this data structure is usually the same for dark and light images.

A high-pass filter is then applied to the image to remove the low-frequency components of the image and the high-frequency components, i.e., image details such as corners and the boundary between light and dark color intensities, become more visible. These filters can be applied as Gaussian, averaging, or Rolling Guidance Filter (RGF). Therefore, the final transmission is expressed as Equation 11.

$$t(x) = low - pass\ filter\ (t'(x)) \quad (11)$$

3.5. Recovering the Natural Image in All Three-Color Channels

In the last preprocessing step, and after the calculating the atmospheric light and transmittance map, the original image inverted J_{inv}^{c} can be recovered from the output of the previous step by removing the extra atmospheric light using Equation 12:

$$J_{inv}^{c} = \frac{(I_{inv}^{c} - A^{c})}{t(x)} + A^{c} \quad (12)$$

In Equation 12, I_{inv}^{c} are the inverted image components in all three channels R, G, and B. A^{c} is the value of atmospheric light, and t(x) is the transmission function based on low-pass noise-removal filters (Equation 11). Fig. 10 shows an example output image of a reconstructed GAN network.

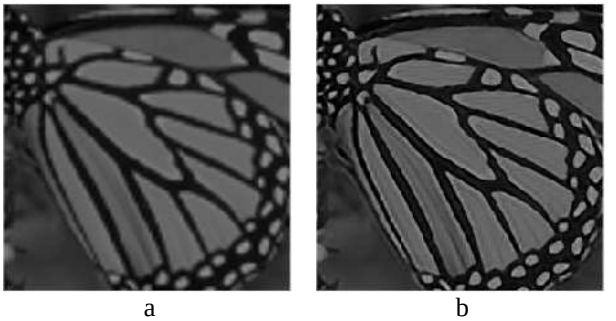

a b

Fig. 10. a) Removing artificial light from the input image b) Reconstructed image by GAN.

3.6. Importing the Enhanced LR Image to the SRGAN and Converting it to an SR Image

In this step, the pre-processed LR image enters to the G network for generating an SR image. The G network uses some convolutional layers and has a special architecture, called Resnet. In this network, the ReLU activation function is used after each convolution layer. The image in the Resnet passes through two convolutional layers and the output is aggregated with the input to compensate the image details, which are lost through the convolution layers. Residual blocks in the Resnet create 64 feature maps from each image. After each convolutional layer, a Batch Normalization (BN) process is performed to improve the network training process. The output from the Resnet network passes through a convolutional layer with 64 feature maps and step 1 to normalize the data and then, this output is added to the first layer output. Finally, the SR image is created with the final convolutional layer.

3.7. Evaluating the Quality of SR Image by the D network

In this step, the SR image created in the previous step is given to the D network. This network uses 8 convolutional layers and VGG54 architecture. In the first layer, the image passes through a convolutional layer with 64 feature maps and step 1. In D network, the LeakyRelu activation function is used after each convolutional layer. From the second layer onwards, the BN process is performed and the feature maps are doubled to reach 512 feature maps. Doubling feature maps is a characteristic of the VGG network. Finally, a reconstructed image is created using the Sigmoid function.

3.8. Testing the Final Goal of SR Operation

In the final step, the D network detects that the image is SR or not. If the image is an SR, the method has reached to its target. Otherwise, the generated SR image in the previous step will be returned to the G network so that the network will be trained again. The re-trained image is then fed to the D network to re-evaluate the image quality. This process continues until the image becomes SR. Fig. 11 shows an example SR image, which is, has been created by the above method.

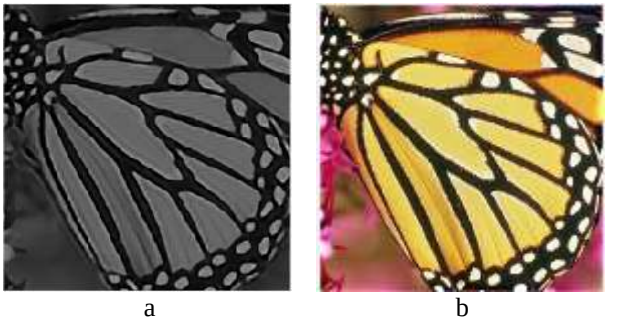

a b

Fig. 11. a) The output of the reconstructed image by the GAN b) SR output

4. RESULTS

The use of dark channels along with luminance maps allows the artificial light of an image to be removed and the atmospheric light to be retained as the main part of the image. In other words, the proposed method acts as a preprocessing phase (normalization) of GAN networks and ultimately leads to an increase in the final image quality.

Here, the simulation results are presented in two phases of preprocessing and final processing. The hardware used in this study was a 5-core processor with a speed of 3.3 GHz, 16 GB RAM, 2 GB of graphical memory, and a Windows 10 operating system.

4.1. Pre-processing Phase Results

After receiving an LR image, its dark channels are found and its artificial atmospheric light is removed by applying a Laplacian filter and initializing the atmospheric light. The important point is selecting the proper size of the neighborhood window in dark channels, the parameter ω in the conversion function, and the value of initial atmospheric light, which have a direct impact on the final output of the model. If these parameters are selected large, the image becomes artificial and we will see the noise even when the Laplacian noise removal filter is applied. If these parameters are considered small, in addition to increasing the processing time, the dynamic range of the image will be affected and the image quality will be decreased. The values of the parameters ω and atmospheric light are between zero and one. These parameters are used in the transmission function and in luminance maps [15]. Window size is also an odd number greater than 3.

According to [15], in this paper, window sizes was selected 15 pixels, the value of atmospheric light was selected to the maximum brightness of the pixels of the image corresponding to 0.1% of the maximum brightness of the luminance map, and the value of

parameter ω in the conversion function equal was selected to 0.98. Examples of outputs from the preprocessing phase are shown in Figs. 12, 13, and 14 for the Set5, Set14, and BSD100 databases, respectively.

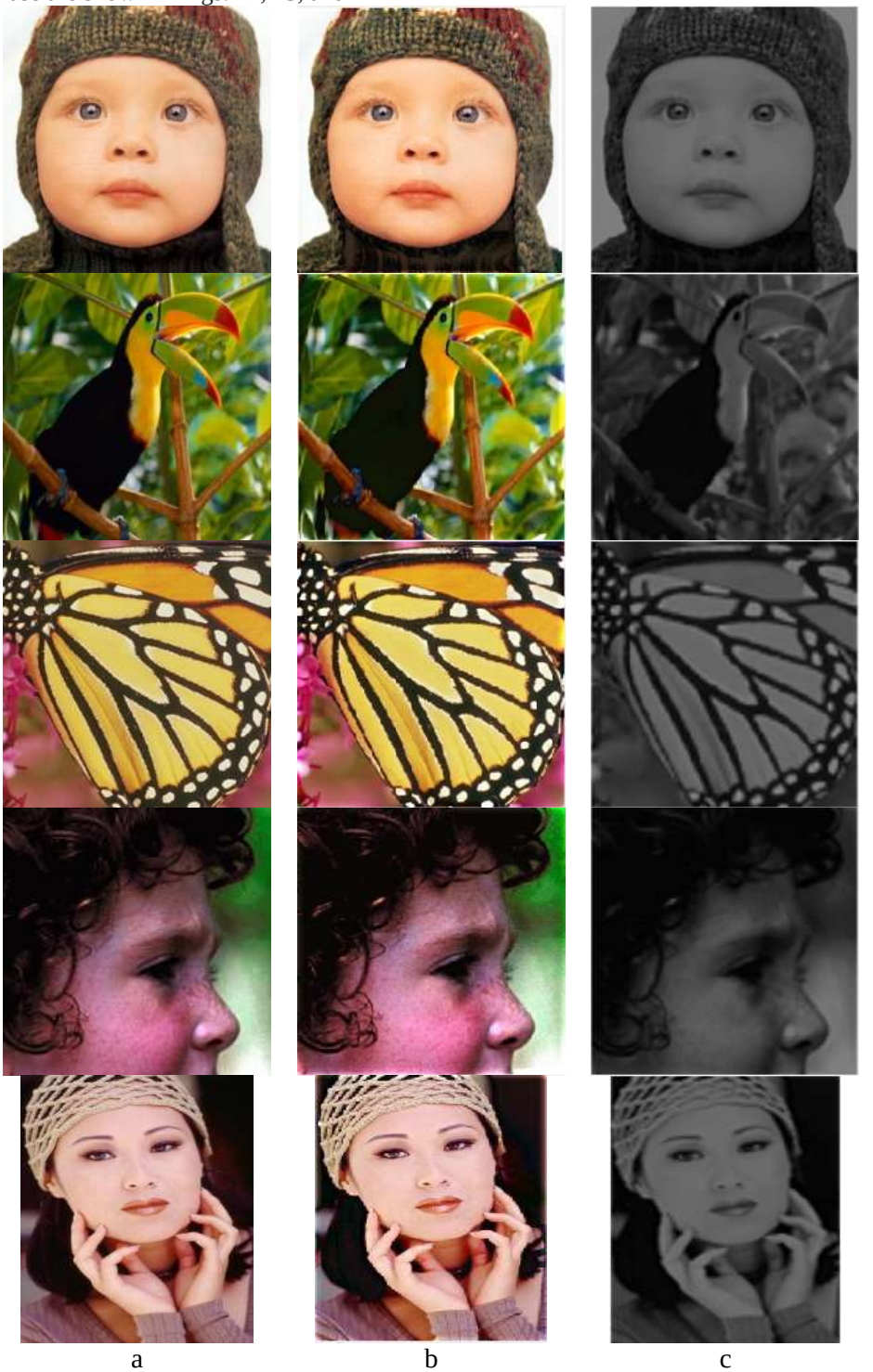

Fig. 12. Set5 database images a) The LR input image b) Atmospheric light calculation by using dark channels c) Elimination of artificial light for the input image

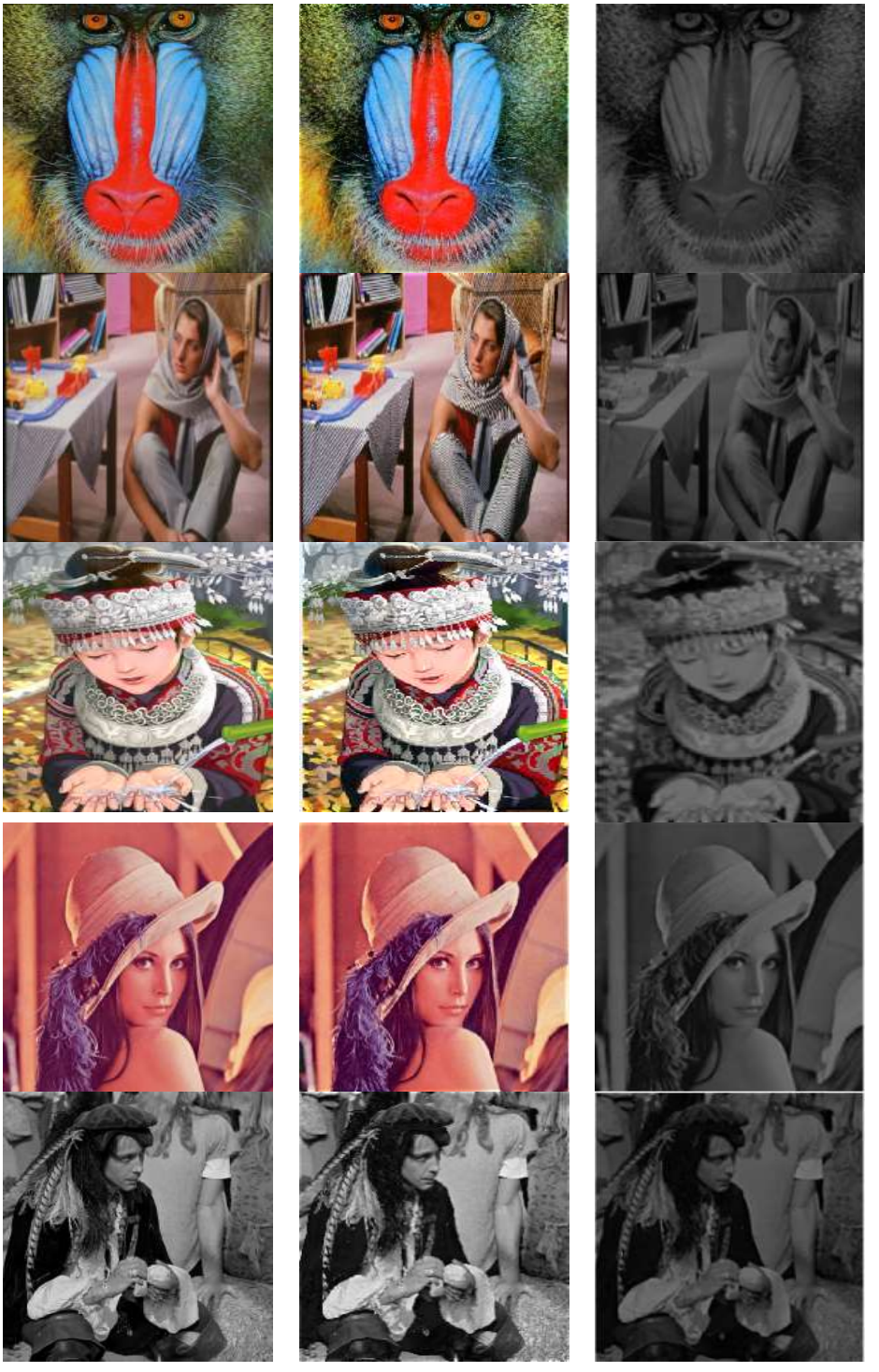

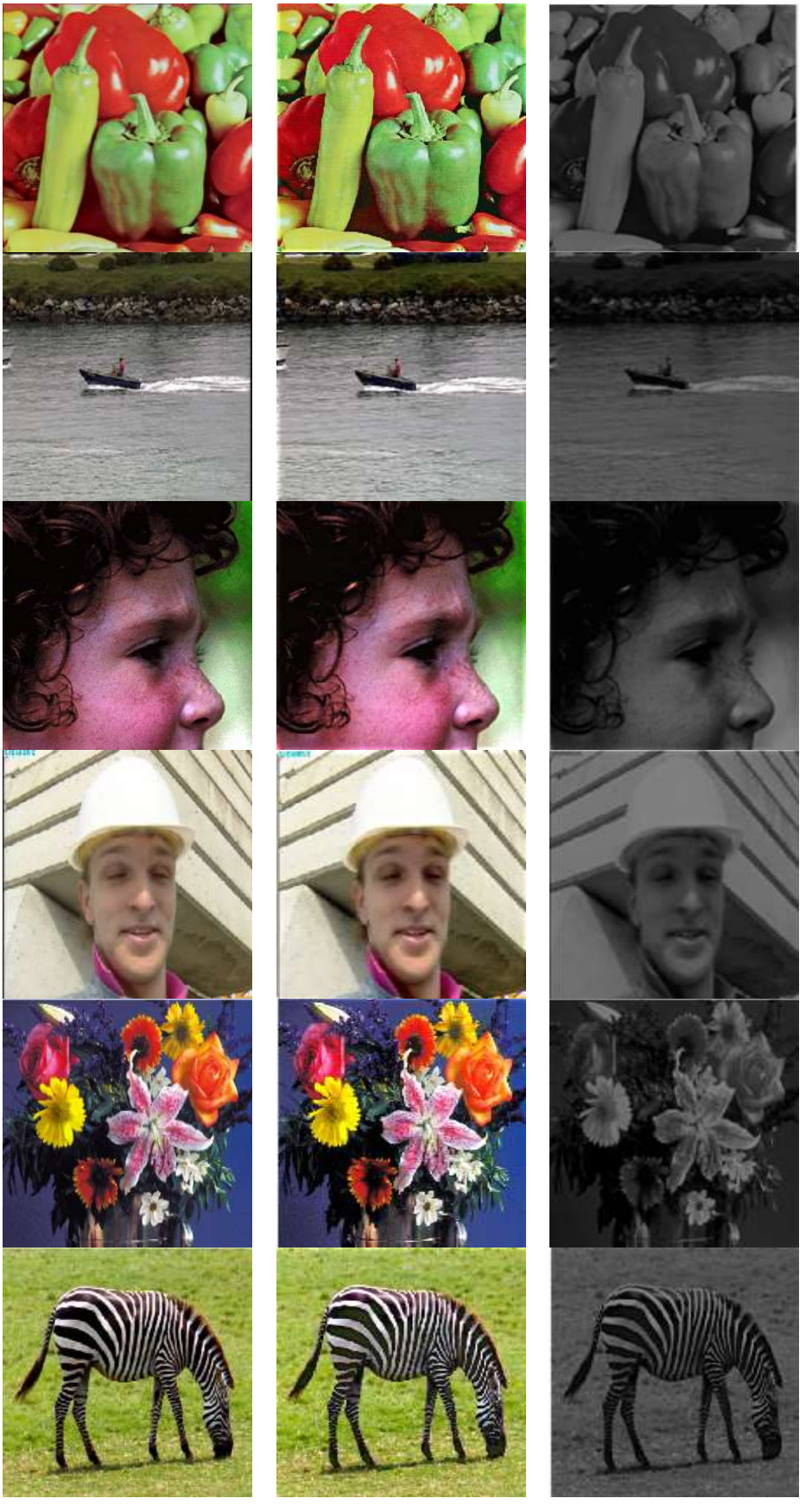

a b c

Fig. 13. Set14 database images a) The LR input image b) Atmospheric light calculation by using dark channels c) Elimination of artificial light for the input image.

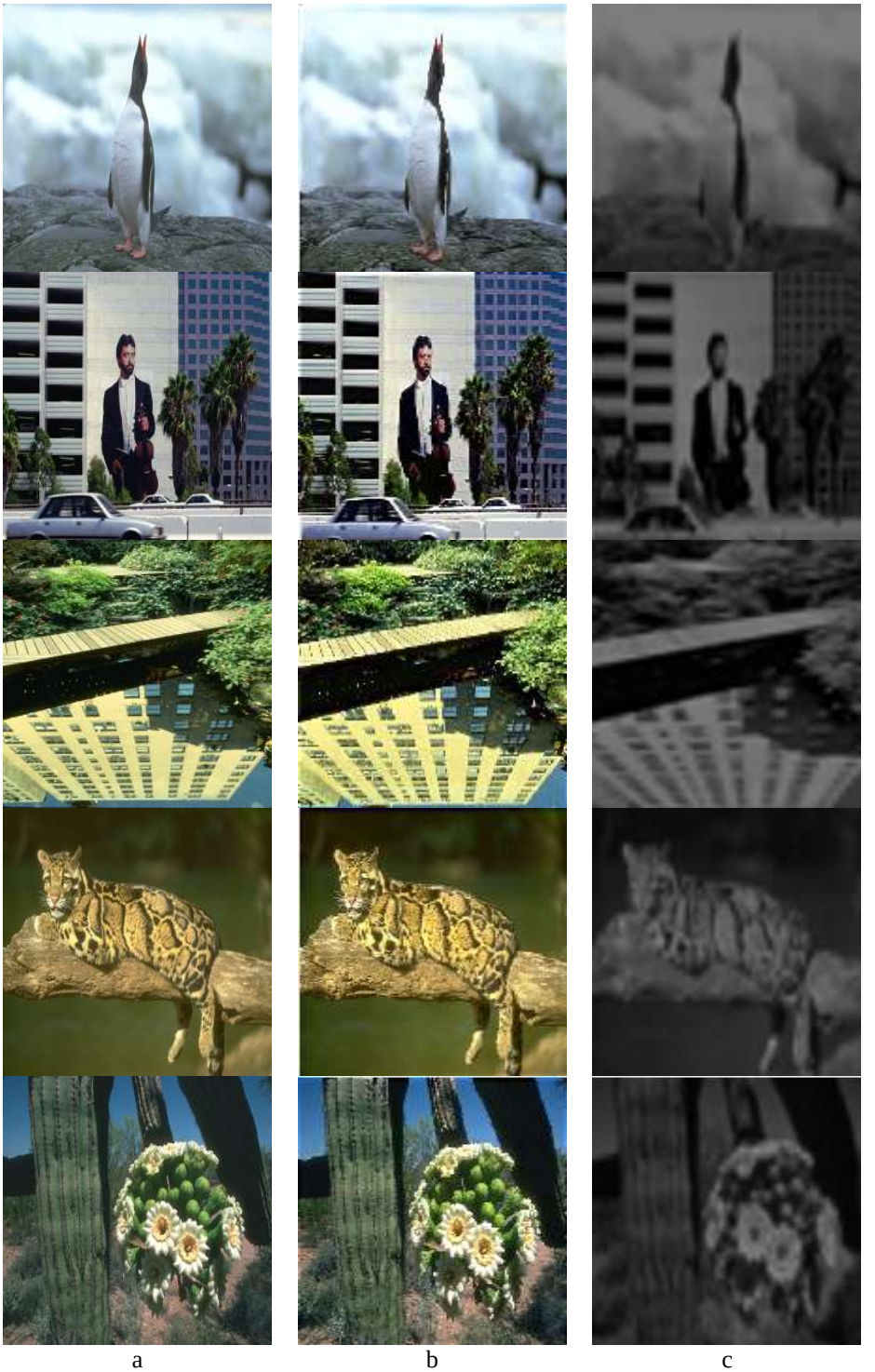

a b c

Fig. 14. BSD100 database images a) The LR input image b) Atmospheric light calculation by using dark channels c) Elimination of artificial light for the input image.

4.2. The Final Output of the Model

After removing the atmospheric light, the image is provided to the GAN neural network. At this stage, the G and D networks produce an HR image and repeat this process until they reach the maximum possible quality. Fig. 15 shows an example of the final output of the proposed model.

a b

Fig. 15. a) An example of an input LR image b) The final output of the model.

As shown in Fig. 15, the image quality has been improved after removing atmospheric light and reproducing in the GAN neural network. This shows the success of the model in providing HR images. Figs. 16, 17, and 18 show the outputs model by using Set5, Set14, and BSD100 databases, respectively.

a b

Fig. 16. Set5 database images a) Input LR image b) Final SR image.

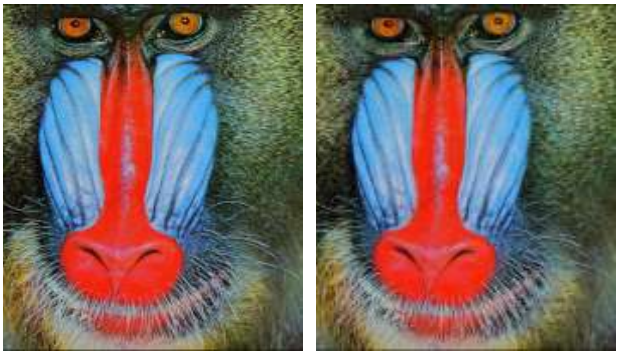

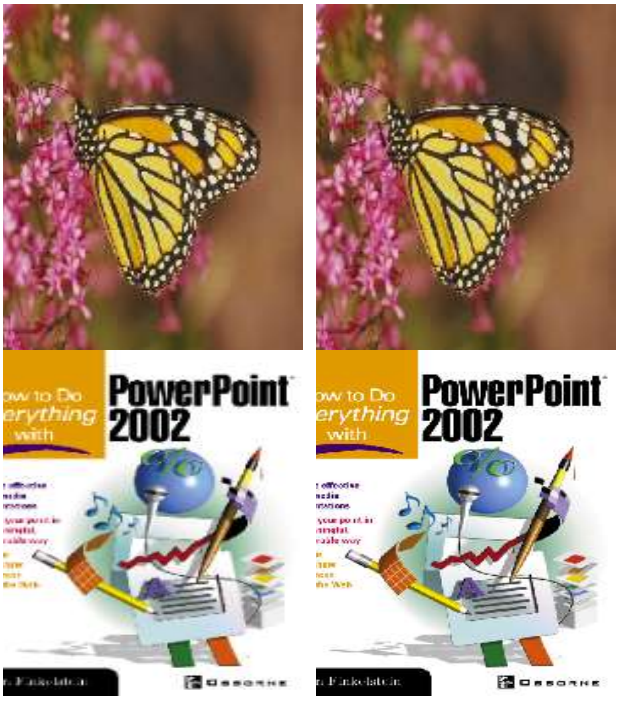

a b

Fig. 17. Set14 database images a) Input LR image b) Final SR image.

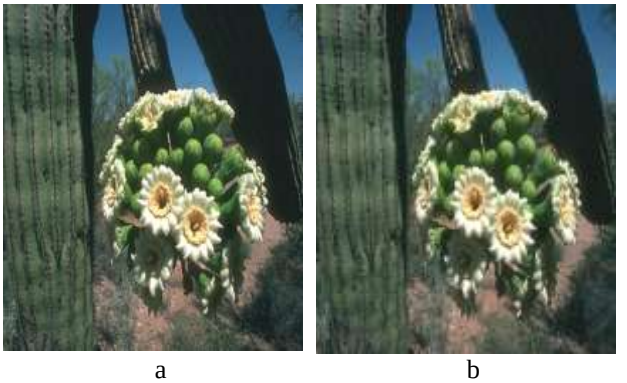

a b

Fig. 18. BSD100 database images a) Input LR image b) Final SR image

Fig. 19 shows only small parts of some LR sample images from employed benchmark datasets, and generated HR images after applying the proposed preprocessing method. As shown in this figure, the proposed preprocessing approach has improved the image quality, significantly.

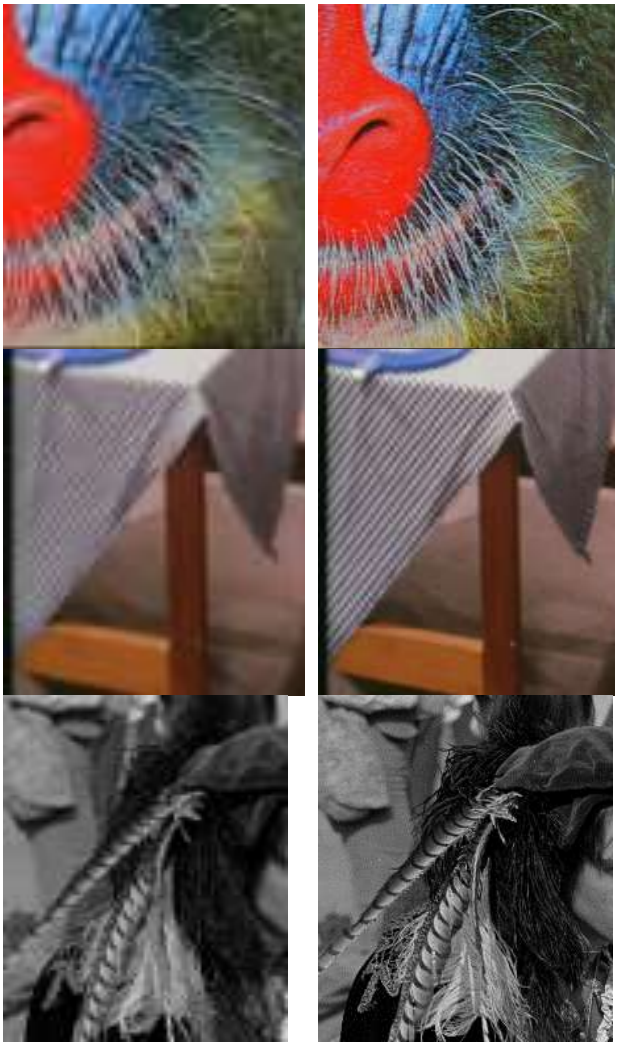

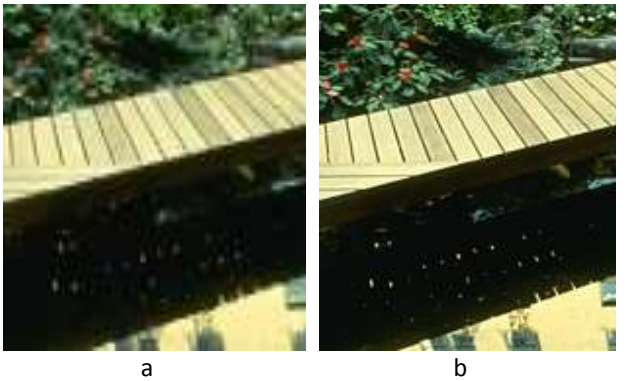

a b

Fig. 19. Parts of Sample images a) Input LR image b) Final SR image

4.3. Quantitative Evaluation of the Results

Similar to most rival methods in the field, the evaluation parameters of the proposed model are SSIM and PSNR, the maximum value of which will be considered. Tables 1, 2, and 3 show the quality obtained based on SSIM and PSNR parameters. The image's number in these tables corresponds to the number of the images in Figs. 16, 17, and 18, which are related to Set5, Set14, and BSD100 databases.

Table 1. SSIM and PSNR criteria values for Set5 database images (4x upscaling).

Image #	PSNR	SSIM
1	36.8719	**0.927935**
2	35.4232	**0.936712**
3	27.3130	**0.845767**
4	36.0836	**0.869826**
5	32.1025	**0.910368**

Table 2. SSIM and PSNR criteria values for Set14 database images (4x upscaling).

Image #	PSNR	SSIM
1	26.4862	**0.612112**
2	29.5713	**0.795379**
3	30.1589	**0.882658**
4	35.1125	**0.905991**
5	33.5480	**0.918725**
6	35.9081	**0.915577**
7	29.8586	**0.705866**
8	35.9970	**0.868933**
9	34.7770	**0.926041**
10	30.4462	**0.836585**
11	29.9918	**0.829732**
12	32.7433	**0.936745**
13	28.2287	**0.895181**

Table 3. SSIM and PSNR criteria values for BSD100 database images (4x upscaling).

Image #	PSNR	SSIM
1	27.3461	**0.643445**
2	29.8407	**0.837625**
3	33.6474	**0.888125**
4	35.9148	**0.920552**
5	27.0329	**0.751527**
6	25.4055	**0.705152**
7	30.6426	**0.863099**
8	30.0987	**0.787296**

The images in the used datasets have various challenges such as atmospheric light and noise. However, the results in Tables 2, 3, and 4 indicate that the proposed method has achieved appropriate values for the SSIM and PSNR parameters.

5. COMPARISON RESULTS

In this section, the outputs obtained from the proposed model have been compared with the rival methods ElapcGAN [25], CGAN [26], GDSR [28], and SeaNet [37]. In all of these sources, the same datasets have been used.

Table 4 shows the mean obtained from the PSNR and SSIM performance evaluation parameters on the Set5, Set14, and BSD100 datasets. In addition, Table 5 shows the percentage improvement of the PSNR and SSIM parameters by comparing the results of the proposed method and the best results in the research literature (SeaNet method [37] and ElapCGAN method [25]). Yellow cells show the values obtained from this study and blue cells show the closest results from the competing methods.

Table 4. Values of quality evaluation parameters PSNR and SSIM (4x upscaling).

Method	Set5		Set14		BSD100	
	PSNR	SSIM	PSNR	SSIM	PSNR	SSIM
SRGAN [24]	29.40	0.8472	26.02	0.7397	25.16	0.6688
ELapCGAN [25]	32.16	0.8970	28.61	0.7960	27.69	0.7410
CGAN [26]	32.15	0.8946	28.62	0.7841	27.66	0.7394
GDSR [27]	30.93	0.8641	27.56	0.7723	26.02	0.6782
SeaNet [37]	32.33	0.8970	28.72	0.7855	27.65	0.7388
The Proposed model	33.56	0.8990	31.77	0.8207	29.99	0.7996

Table 5. Percentage improvement of SSIM and PSNR parameters.

	Set5 (%)	Set14 (%)	BSD100 (%)
PSNR	4.35	10.62	**8.31**
SSIM	0.23	3.10	**7.91**

6. CONCLUSION AND DISCUSSION

By comparing the quality of the output images of the proposed model with other SR methods, it is seen that the proposed method has experienced an increase in quality compared to competing models. The proposed method achieved more quality images compared with rival methods, by dynamically selecting the parameters of mapping and extraction of atmospheric light. Generally, choosing the right size of dark channels is very important. The dark channels select a radius of *n* pixels in their neighborhood and then select the lowest color intensity. The proper size of dark channels is the value of the parameter *n* so that if this parameter is considered large, it will lead to artificialization and problems such as halo (reduction of the dynamic level of the image). If the parameter *n* is considered small, the number of image slices will increase and the time required to process LR images will increase, significantly. The choice of window size 15 in this article, based on the research of Song et al. [15], has prevented the above problems.

For the Set5 database, the average maximum mean values of PSNR and SSIM are 33.56 and 0.8990, respectively, belonging to the proposed model. In addition, in using the Set14 database, these parameters belong to the proposed model with 31.7695 and 0.8207, respectively. The same was true for the BSD100 dataset with the average maximum mean values of PSNR and SSIM parameters of 29.9910 and 0.7996, respectively, related to the proposed method.

The main advantages of the proposed method include the following:

1. Providing better accuracy in increasing image quality compared with GAN neural networks.
2. Reducing the sensitivity of the proposed operation to noise due to the use of a softening filter in the transmission function.
3. Eliminating the artificial lights using luminance maps that increases the quality of the final output. Artificial lights are masks of color intensities that are placed on the image and cause a change in its dynamic range.

The proposed method in this paper is based on dark channels and luminance maps. Proper selection of dark

channel windows sizes is one of the main challenges of this method so that in different images, a fixed value cannot be assigned to them. In addition, the amount of light in dark channels, in indoor images, is almost zero. This fact causes the selection of the lowest color intensity in the neighborhood of the input pixels to lose its efficiency, in practice. In addition, in this situation, the proposed algorithm will be a time-consuming process [37]. As future solutions, applying inverting filters on input images with a point spread function can be used to remove artificial light. This process, in addition to reducing the order of time, can lead to a reduction in noise sensitivity and ultimately increase the quality of the final output.

CONFLICT OF INTEREST

The authors confirm that there is no conflict of interest.

FUNDING INFORMATION

There is no funding for this paper.

REFERENCES

[1] Burger W, Burge MJ. "**Digital image processing: an algorithmic introduction using Java**". *Springer*; 2016.

[2] Huang S, Sun J, Yang Y, Fang Y, Lin P, Que Y. "**Robust single-image super-resolution based on adaptive edge-preserving smoothing regularization**". *IEEE Transactions on Image Processing*, Vol. 27(6), pp. 2650-2663, 2018. http://doi.org/ 10.1109/TIP.2018.2809472

[3] Yue L, Shen H, Li J, Yuan Q, Zhang H, Zhang L. "**Image super-resolution: the techniques, applications, and future**". *Signal Processing 2016*, **128**, pp. 389-408, 2016. https://doi.org/10.1016/j.sigpro.2016.05.002

[4] Haris M, Watanabe T, Fan L, Widyanto MR, Nobuhara H. "**Super resolution for UAV images via adaptive multiple sparse representation and its application to 3-d reconstruction**". *IEEE Transactions on Geoscience and Remote Sensing 2017*, **55(7)** , pp. 4047-4058, 2017. http://doi: 10.1109/TGRS.2017.2687419

[5] Ayas S, Ekinci M. "**Learning based single image super resolution using discrete wavelet transform**". *In international conference on computer analysis of images and patterns*, pp. 462-472, Springer, cham; 2017.

[6] Waleed Gondal M, Scholkopf B, Hirsch M. "**The unreasonable effectiveness of texture transfer for single image super-resolution**". *In Proceedings of the European Conference on Computer Vision (ECCV) 2018*, pp. 80-97, Springer, Cham.

[7] Lei J, Zhang S, Luo L, Xiao J, Wang H. "**Super-resolution enhancement of UAV images based on fractional calculus and POCS**". *Geo-spatial information science 2018*, **21(1)**, pp. 56-66, 2018. https://doi.org/10.1080/10095020.2018.1424409

[8] Liu H, Fu Z, Han J, Shao L, Liu H. "**Single satellite imagery simultaneous super-resolution and colorization using multi-task deep neural networks**". *Journal of visual communication and image representation 2018*, **53**, pp**.** 20-30, 2018. https://doi.org/10.1016/j.jvcir.2018.02.016

[9] Han W, Chu J, Wang L, Pan C. "**Edge-directed single image super-resolution via cross-resolution sharpening function learning**". *Multimedia tools and applications 2017*, **76(8**), pp. 11143-11155, 2017. https://doi.org/10.1007/s11042-016-3656-z

[10] Bei Y, Damian A, Hu S, Menon S, Ravi N, Rudin C. "**New techniques for preserving global structure and denoising with low information loss in single-image super-resolution**". In *the IEEE conference on computer vision and pattern recognition (CVPR) workshops 2018,* pp. 874-881, 2018.

[11] Brifman A, Romano Y, Elad M. "**Unified Single-Image and Video Super-Resolution via Denoising Algorithms**". *IEEE Transactions on Image Processing 2019*, **28(12),** pp. 6063-6076, 2019. http://doi.org/10.1109/TIP.2019.2924173.

[12] Ding N, Liu YP, Fan LW, Zhang CM. "**Single Image Super-Resolution via Dynamic Lightweight Database with Local-Feature Based Interpolation**". *Journal of Computer Science and Technology 2019*, **34(3),** pp. 537-549, 2019. https://doi.org/10.1007/s11390-019-1925-9

[13] Yang W, Zhang X, Tian Y, Wang W, Xue JH, Liao Q. "**Deep learning for single image super-resolution: A brief review**". *IEEE Transactions on Multimedia 2019*, **21(12),** pp. 3106-3121. http://doi.org/10.1109/TMM.2019.2919431

[14] Lu H, Li Y, Nakashima S, Serikawa S. "**Single image dehazing through improved atmospheric light estimation**". *Multimedia Tools and Applications 2016*, **75(24),** pp. 17081-17096. https://doi.org/10.1007/s11042-015-2977-7

[15] Song J, Zhang L, Shen P, Peng X, Zhu G**. "Single low-light image enhancement using luminance map**". In *Chinese Conference on Pattern Recognition 2016*, pp. 101-110. Springe**r,** Singapore. https://doi.org/10.1007/978-981-10-3005-5_9

[16] Goodfellow I, Pouget-Abadie J, Mirza M, Xu B, Warde-Farley D, Ozair S, Bengio Y. "**Generative adversarial nets**". In *Advances in neural information processing systems 2014*, pp. 2672-2680, 2014.

[17] Chang HW, Zhang Q W, Wu QG, Gan Y. "**Perceptual image quality assessment by independent feature detector**". *Neurocomputing 2015*, **151**, pp. 1142-1152. https://doi.org/10.1016/j.neucom.2014.04.081

[18] Tuna C, Unal G, Sertel E. "**Single-frame super resolution of remote-sensing images by convolutional neural network**s". *International Journal of Remote Sensing 2018*, **39(8),**pp. 2463-2479.https://doi.org/10.1080/01431161.2018.1425561

[19] Li F, Xin L, Guo Y, Gao J, Jia X. "**A framework of mixed sparse representations for remote sensing images**". *IEEE Transactions on Geoscience and Remote Sensing 2017*, **55(2),** pp. 1210-1221. http://doi.org/10.1109/TGRS.2016.2621123

[20] Fan C, Wu C, Li G, Ma J. "**Projections onto convex sets super-resolution reconstruction based on point spread function estimation of low-resolution remote sensing images**". *Sensors 2017*, 17(2), pp. 362. https://doi.org/10.3390/s17020362

[21] Lv Z, Jia Y, Zhang Q. "**Joint image registration and point spread function estimation for the super-resolution of satellite images**". *Signal processing: image communication 2017*, **58,** pp. 199-211. https://doi.org /10.1016/j.image. 2017. 08.006

[22] Cruz C, Mehta R, Katkovnik V, Egiazarian KO. "**Single image super-resolution based on wiener filter in similarity domain"**. *IEEE Transactions on Image Processing 2018*, **27(3),** pp. 1376-1389. http://doi.org/10.1109/TIP.2017.2779265

[23] Lin G, Wu Q, Chen L, Qiu L, Wang X, Liu T, Chen X. "**Deep unsupervised learning for image super-resolution with generative adversarial network**". *Signal Processing: Image Communication 2018*, **68,** pp. 88-100. https://doi.org/10.1016/j.image.2018.07.003

[24] Ledig C, Theis L, Huszár F, Caballero J, Cunningham A, Acosta A, Shi W. "**Photo-realistic single image super-resolution using a generative adversarial network**". In *Proceedings of the IEEE conference on computer vision and pattern recognition 2017*, pp. 4681-4690.

[25] Zhang X, Song H, Zhang K, Qiao J, Liu Q. "**Single image super-resolution with enhanced Laplacian pyramid network via conditional generative adversarial learning**". *Neurocomputing 2020*, **398,** pp. 531-538. https://doi.org/10.1016/ j.neucom .2019.04.097

[26] Qiao J, Song H, Zhang K, Zhang X. "**Conditional generative adversarial network with densely-connected residual learning for single image super-resolution**". *Multimedia Tools and Applications 2021*, **80(3),** pp. 4383-4397. https://doi.org/10.1007/s11042-020-09817-2

[27] Chen W, Liu C, Yan Y, Jin L, Sun X, Peng X. "**Guided Dual Networks for Single Image Super-Resolution**". *IEEE Access 2020*, **8** :93608-93620. doi: 10.1109/ACCESS.2020.2995175.

[28] Haris M, Shakhnarovich G, Ukita N. "**Deep Back-Projection Networks for Single Image Super-resolution**". *IEEE Transactions on Pattern Analysis and Machine Intelligence 2019*, **43(12),** pp. 4323-4337. http://doi.org/10.1109/ TPAMI.2020.3002836

[29] Hu Y, Li J, Huang Y, Gao X. "**Channel-wise and spatial feature modulation network for single image super-resolution**". *IEEE Transactions on Circuits and Systems for Video Technology 2019*, **30(11),** pp. 3911-3927. http://doi.org/10.1109/ TCSVT.2019.2915238

[30] Xu X, Li X. SCAN: "**Spatial Color Attention Networks for Real Single Image Super-Resolution**". *In Proceedings of the IEEE Conference on Computer Vision and Pattern Recognition Workshops 2019*.

[31] Gao S, Zhuang X. "**Multi-scale deep neural networks for real image super-resolution**". In *proceedings of the IEEE conference on computer vision and pattern recognition workshops 2019.*

[32] Xie C, Liu Y, Zeng W, Lu X. "**An improved method for single image super-resolution based on deep learning**". *Signal, image and video processing 2019*, **13(3)** :557-565. https://doi.org/10.1007/s11760-018-1382-x

[33] Yang W, Wang W, Zhang X, Sun S, Liao Q. "**Lightweight feature fusion network for single image super-resolution**". *IEEE Signal Processing Letters 2019*, **26(4),** pp. 538-542. http://doi.org/10.1109/LSP.2018.2890770

[34] Dai T, Cai J, Zhang Y, Xia ST, Zhang L. "**Second-order attention network for single image super-resolution**". In *proceedings of the IEEE Conference on Computer Vision and Pattern Recognition 2019*, pp. 11065-11074.

[35] Wang Y, Wang L, Wang H, Li P. "**End-to-end image super-resolution via deep and shallow convolutional networks**". *IEEE Access 2019*, **7,** pp. 31959-31970. http://doi.org/10.1109 /ACCESS.2019.2903582

[36] Xu W, Chen R, Huang B, Zhang X, Liu C. "**Single image super-resolution based on global dense feature fusion convolutional network**". *Sensors 2019*, **19(2),** pp. 316. https://doi.org/10.3390 /s19020316

[37] Fang F, Li J, Zeng T. "**Soft-Edge Assisted Network for Single Image Super-Resolution**". *IEEE Transactions on Image Processing 2020*, **29,** pp. 4656-4668. http://doi.org/10.1109/TIP.2020.2973769

[38] https://deepai.org/dataset/set5-super-resolution (Accessed 20 May 2022)

[39] https://deepai.org/dataset/set14-super-resolution (Accessed 20 May 2022)

[40] https://deepai.org/dataset/bsd100-4x-upscaling (Accessed 20 May 2022)

[41] Guo X, Li Y, Ling H. "**LIME: Low-light image enhancement via illumination map estimation**". *IEEE Transactions on Image Processing 2017*, **26(2),** pp. 982-993. http://doi.org/10.1109/TIP.2016.2639450